

A stars-gas dual fit result in the ‘constant Lagrangian’ model for galactic dynamics when applied to the SPARC database.

E.P.J. de Haas^{1, a)}

Nijmegen, The Netherlands

(Dated: April 24, 2018)

In this paper I apply the ‘constant Lagrangian’ model for galactic dynamics to a subset of the SPARC database. I will fit 25 galaxies from this database using the dual fit approach. This means that one fit is made for the stars dominated region of one galaxy. Another fit is added for the gas dominated region of the same galaxy. Both are presented in one single graph. The switch from stars dominated to gas dominated is sometimes visible as a “wobble” in the total rotation velocity, as for example in the rotation curve of NGC 1560. I will demonstrate that this more or less visible “wobble” is part of the rotation velocity curve of almost every galaxy in the sample. The dual fit approach results in a rotation curve fit that mostly remains within the observational error margins.

PACS numbers: 95.30.Sf, 95.35.+d

Keywords: Dark Matter, MOND, Schwarzschild, Galactic rotation curves

^{a)}Electronic mail: haas2u@gmail.com

CONTENTS

I. Introduction	3
II. The ‘constant Lagrangian’ model for galactic dynamics	3
III. The stars to gas “wobble” in the rotation curve of NGC 1560	8
IV. The stars to gas shift in the rotation curve of some other galaxies	12
V. Some more rotation curve fits: F583-1, F579V1 and U11648	24
References	39

I. INTRODUCTION

In a previous paper I introduced the ‘constant Lagrangian’ model for galactic dynamics (de Haas, 2018a). In two sub-sequential papers I made a first qualitative attempt at fitting real rotational velocity curves using the proposed model (de Haas, 2018c,b). In this paper I will give a more quantitative analysis by including the error bars of the measured velocity. This approach will be applied to a subset of 25 galaxies of the [SPARC database](#), including the error margins, as provided by (Lelli et al., 2016).

II. THE ‘CONSTANT LAGRANGIAN’ MODEL FOR GALACTIC DYNAMICS

I start by repeating the essentials of this model, which I then apply to the rotation curve of galaxy NGC 1560. The Lagrangian equation of motion reads

$$\frac{d}{dt} \left(\frac{\partial L}{\partial \dot{q}} \right) - \frac{\partial L}{\partial q} = 0. \quad (1)$$

In classical gravitational dynamics I assume circular orbits with $\dot{q} = v$ and $q = r$. The Lagrangian itself is then given by $L = K - V$, with V the Newtonian potential gravitational energy and K the kinetic energy. One then gets

$$\frac{d}{dt} \left(\frac{\partial L}{\partial \dot{q}} \right) = \frac{dp}{dt} = F. \quad (2)$$

The other part gives

$$\frac{\partial L}{\partial q} = -\frac{dV}{dr}, \quad (3)$$

so one gets Newton’s equation of motion in a central field of gravity

$$F_g = -\frac{dV}{dr}. \quad (4)$$

Further analysis of the context results in the identification of the Hamiltonian of the system, $H = K + V$, as being a constant of the orbital motion and the virial theorem as describing a relation between K and V in one single orbit but also between different orbits, $2K + V = 0$.

The previous analysis is problematic relative to the notion of geodetic motion in General Relativity. The problem can best be described in a semi-relativistic approach using the classical Lagrangian equation of motion for geodetic orbits. The most important aspect of

geodetic motion in GR is that it requires no force to move on a geodetic. This has important implications for the Lagrangian equation of motion, because $F = 0$ on a geodetic. One gets

$$\frac{d}{dt} \left(\frac{\partial L}{\partial \dot{q}} \right) = F_g = 0 \quad (5)$$

and as a consequence also

$$\frac{\partial L}{\partial q} = -\frac{dL}{dr} = 0. \quad (6)$$

As a result, one gets the crucial

$$L = K - V = \text{constant} \quad (7)$$

on geodetic orbits.

This result, the Lagrangian of the system as being the constant of the geodetic motion, is used on a daily basis by many of us because it is used by GNSS systems for the relativistic correction of atomic clocks in their satellites. Let's elaborate this a bit further. If we apply the Schwarzschild metric in polar coordinates, we have (Ruggiero et al., 2008)

$$ds^2 = \left(1 + \frac{2\Phi}{c^2} \right) c^2 dt^2 - \left(1 + \frac{2\Phi}{c^2} \right)^{-1} dr^2 - r^2 d\theta^2 - r^2 \sin^2 \theta d\phi^2. \quad (8)$$

In case of a clock on a circular geodesic on the equator of a central non-rotating mass M we have $\frac{dr}{dt} = 0$, $\frac{d\theta}{dt} = 0$, $\sin\theta = 1$ and $\frac{d\phi}{dt} = \omega$. We thus get, with $v_{orbit} = r\omega$, the GR result

$$\frac{d\tau}{dt} = \sqrt{1 + \frac{2\Phi}{c^2} - \frac{v_{orbit}^2}{c^2}} \quad (9)$$

with $d\tau$ as the clock-rate of a standard clock A in a geodetic orbit and dt as the 'universal' clock-rate G of a standard clock at rest in infinity, the only condition for which $d\tau = dt$. The result of Eqn. (9) is the basic relativistic correction used in GNSS clock frequencies, with the first as the gravity effect or gravitational potential correction and the second as the velocity effect or the correction due to Special Relativity (Ashby, 2002; Hećimović, 2013; Delva and Lodewyck, 2013).

Given the classical definitions of $K = \frac{mv_{orbit}^2}{2}$ and $V = m\Phi$, we get

$$\frac{d\tau}{dt} = \sqrt{1 - \frac{2L}{U_0}}. \quad (10)$$

All the satellites of a GNSS system are being installed on a similar orbit and thus synchronized relative to one another because they share the same high and velocity and have constant

L and $\frac{d\tau}{dt}$ on those orbits. But different GNSS systems, as for example GPS compared to GALILEO, are functioning on different orbits with different velocities and those systems aren't syntonized relative to one another. This non-syntonization between satellites on orbits with different heights and virial theorem connected velocities is very annoying for the effort towards realizing an integration of the different GNSS systems into one single global network.

Fundamental in the approach of this paper is to analyze gravity using relative frequency shifts, and thus $\frac{d\tau}{dt}$, as one of the basic experimental inputs. Such a method is also looming in today's geodesy. In modern gravitational geodesy scientists are investigating the relativistic frequency shift as a new observable type for gravity field recovery (Mayrhofer and Pail, 2012). Driven by this development, modern geodesy is about to go through a change from the Newtonian paradigm to Einstein's theory of general relativity (Kopeikin et al., 2017). A new generation of atomic clock is the game changer for this new domain of chronometric geodesy, and requires additional new techniques to be developed in the field of frequency transfer and comparison (Delva and Lodewyck, 2013). The paradigm shift towards gravitational divergence recovery is based on the principle of frequency comparison between two clocks on different space-time locations in order to measure the frequency shift between them (Delva and Lodewyck, 2013). The knowledge of the Earth's gravitational field has often been used to predict frequency shifts between distant clocks. In relativistic geodesy, the problem is reversed and the measurement of frequency shifts between distant clocks now provides knowledge of the gravitational field (Delva and Lodewyck, 2013). This reversal also looms in my postulate of the 'constant Lagrangian' model. A constant Lagrangian implies a zero divergence in the syntonization of atomic oscillators and thus an absence of gravitational stress. A divergence in the Lagrangian implies a divergence in the time dilation factor $\frac{d\tau}{dt}$ and thus a non-zero gravitational stress.

The 'constant Lagrangian' model for galactic dynamics starts with the postulate that the geodetic Lagrangian $L = K - V$ is a galactic constant, not just an orbital constant. In this 'time bubble halo' model the classical Newtonian potential is assumed valid. This potential in the case of a model galaxy with a perfect quasi-solid bulge and a perfect Schwarzschild emptiness around it is given in Fig.(1). My model galaxy is build of a model bulge with mass M and radius R and a Schwarzschild metric emptiness around it. The model bulge has constant density $\rho_0 = \frac{M}{V} = \frac{3M}{4\pi R^3}$ and its composing stars rotate on geodetics in a quasi-solid

way. So all those stars in the bulge have equal angular velocity on their geodetic orbits, with $v = \omega r$. On the boundary between the quasi solid spherical bulge and the emptiness outside of it, the orbital velocities are behaving smoothly. So the last star in the bulge and the first star in the Schwarzschild region have equal velocities and potentials. I also assume that the Newtonian potential itself is unchanged and unchallenged, remains classical in the whole galaxy and its surroundings. Such a model galaxy doesn't have a SMBH in the center of its bulge and it only has some very lonely stars in the space outside the bulge.

Point	Relation	Expression
Outside the bulge	$r > R$	$-\frac{GM}{r}$
On the Surface	$r = R$	$-\frac{GM}{R}$
Inside the bulge	$r < R$	$-GM \left[\frac{3R^2 - r^2}{2R^3} \right]$
At the centre	$r = 0$	$-\frac{3}{2} \left(\frac{GM}{R} \right)$

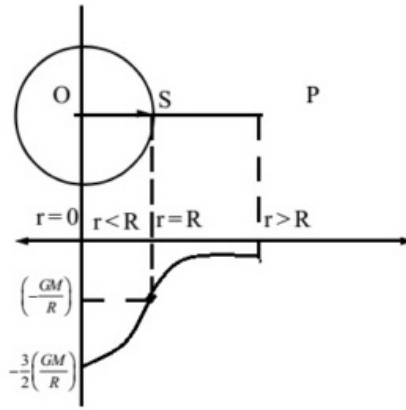


FIG. 1. The potential inside and out of a model bulge

The 'constant Lagrangian model postulates $L = K - V = constant$ in the entire galaxy, without changing the Newtonian potential. As a result, in such a model bulge, L is a constant of the motion, not only in one orbit but also between orbits.

$$\frac{L}{m} = \frac{v_{orbit}^2}{2} + \frac{GM}{r} = \frac{3GM}{2R} = constant. \quad (11)$$

For the region $0 \leq r \leq R$ we get

$$v_{orbit}^2 = \frac{GM}{R} \cdot \frac{r^2}{R^2} \quad (12)$$

and outside the model bulge, where $R \leq r \leq \infty$, we have

$$v_{orbit}^2 = \frac{3GM}{R} - \frac{GM}{r}. \quad (13)$$

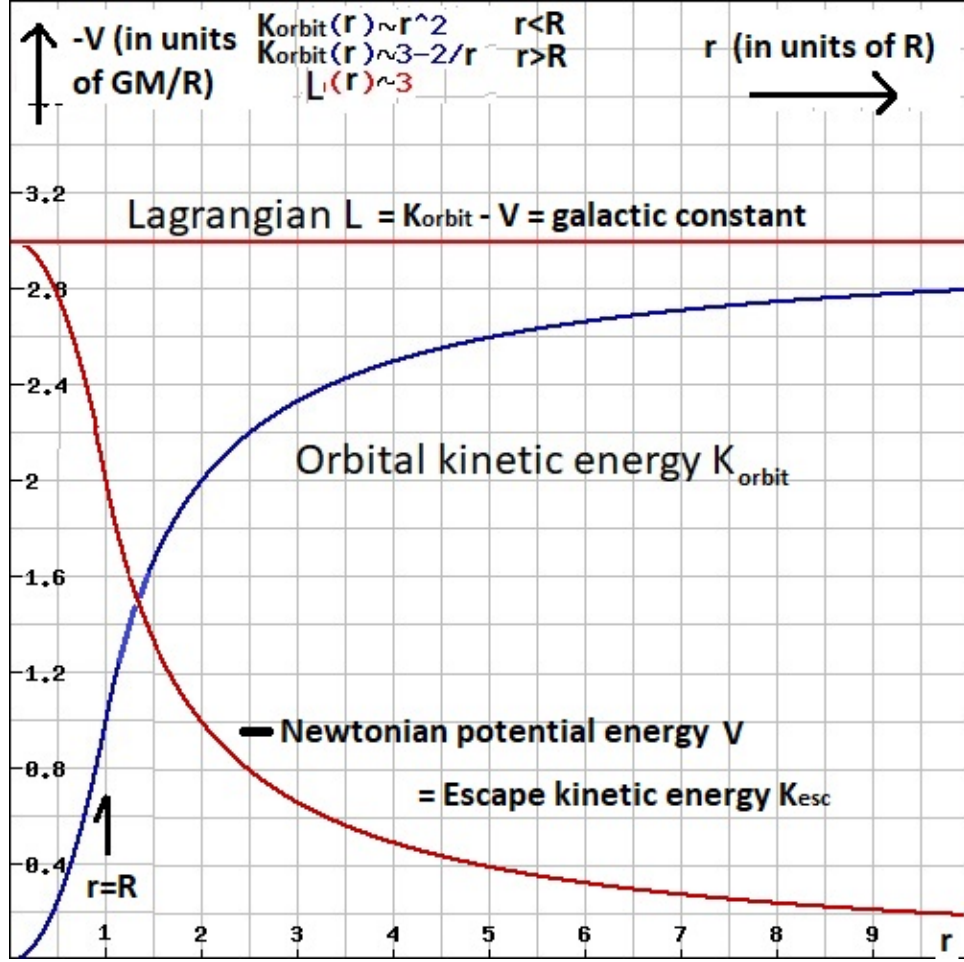


FIG. 2. The square of the orbital velocity profile in the model galaxy with $L = constant$.

From the perspective of a free fall Einstein elevator observer, the free fall on a radial geodesic from infinity towards the center of the bulge, the other free fall tangential geodesics seem to abide the law of conservation of energy, because the escape kinetic energy plus the orbital kinetic energy is a constant on my model galaxy with galactic constant L . An Einstein elevator system with test mass m that would be put in an orbital collapse situation, magically descending from orbit to orbit in a process in thermodynamic equilibrium, would have constant total kinetic energy, from the radial free fall perspective. This can be expressed as $L = K_{orbit} - V = K_{orbit} + K_{escape} = K_{final}$. In Fig.(2) I sketched the result, with $-V = +K_{escape}$.

Such a model galaxy would also be a GNSS engineer's dream come true because the whole model galaxy is in one single synchronized time-bubble.

$$\frac{d\tau}{dt} = \sqrt{1 - \frac{2L}{U_0}}. \quad (14)$$

Given the Baryonic Tully-Fisher relation in Milgrom's version $v_{final}^4 = Ga_0M$ with $2\pi a_0 \approx cH_0$, with a_0 as Milgrom's galactic minimum acceleration and H_0 as the Hubble constant (Milgrom, 1983; McGaugh, 2005), we get as a galactic time bubble fix

$$\frac{d\tau}{dt} = \sqrt{1 - \frac{2L}{U_0}} = \sqrt{1 - \frac{v_{final}^2}{c^2}} = \sqrt{1 - \sqrt{\frac{v_{final}^4}{c^4}}} = \quad (15)$$

$$\sqrt{1 - \sqrt{\frac{Ga_0M}{c^4}}} = \sqrt{1 - \sqrt{\frac{GH_0M}{2\pi c^3}}} = \sqrt{1 - \sqrt{\frac{M}{2\pi M_U}}}, \quad (16)$$

in which I used $L = 3GM/R = K_{final} = \frac{1}{2}mv_{final}^2$ and $M_U = \frac{c^3}{GH_0}$. This last constant can be referred to as an apparent mass of the Universe, a purely theoretical number constant, see (Mercier, 2015).

In a model Universe, this would imply that my model galaxy would be in a proper time bubble with clock-rate $d\tau$ relative to the universal clock-rate dt in proportion to the masses of galaxy M and Universe M_U . In my model galaxy theoretical environment the Baryonic Tully-Fisher relationship implies that the galactic time bubble is fixed through the mass of my model galaxy and that this fix is a cosmological one. So what is a universal acceleration minimum a_0 in MOND can be interpreted as a universally correlated (through M_U) but still local (through M) time bubble fix in my model galaxy geodetic environment. In such a model Universe, the time bubble of a galaxy immediately functions as a gravitational lens, because $\frac{d\tau}{dt}$, as measuring the curvature of the metric, also determines the gravitational index of refraction of the time bubble relative to Cosmic space where $dt = d\tau$. In my model, the Dark Matter halo is above all present as a time bubble halo, determined by the factor $\frac{d\tau}{dt}$.

III. THE STARS TO GAS “WIGGLE” IN THE ROTATION CURVE OF NGC 1560

Having determined the model galactic velocity rotation curve based on the Lagrangian as a galactic constant of orbital motion, the question is to what extent real galaxies can

be modeled in this way. In this section I present the plot of V_{orb}^2 , in $(km/s)^2$ against r , in kpc , with in each plot the experimental values in red stars with vertical error bars and the theoretical values in black circles and black triangles. The fitting plot is with one single fit for M , in units of $10^{10} M_{solar}$, and R , in units of kpc . The most important cut in the model is the change from the model bulge to the model empty space around it. In the model bulge, $V_{orb}^2 \propto r^2$, outside the model bulge $V_{orb}^2 \propto -r^{-1}$.

In the attempt to fit galaxies from the SPARC database, it turned out that the “wobble”, clearly present in the rotation curve of NGC 1560, is a crucial ingredient in most galaxies. This “wobble” in the graph of NGC is described in the following quote.

In the rotation curve of NGC 1560, as derived by B92, there is a clear “wobble” in the total rotation velocity, which corresponds very closely to a similar wobble in the gas contribution to the rotation curve. Mass models such as MOND naturally reproduce the feature, whereas models that include a dominant spherical (or triaxial) halo are too smooth to do so. (Gentile et al., 2010)

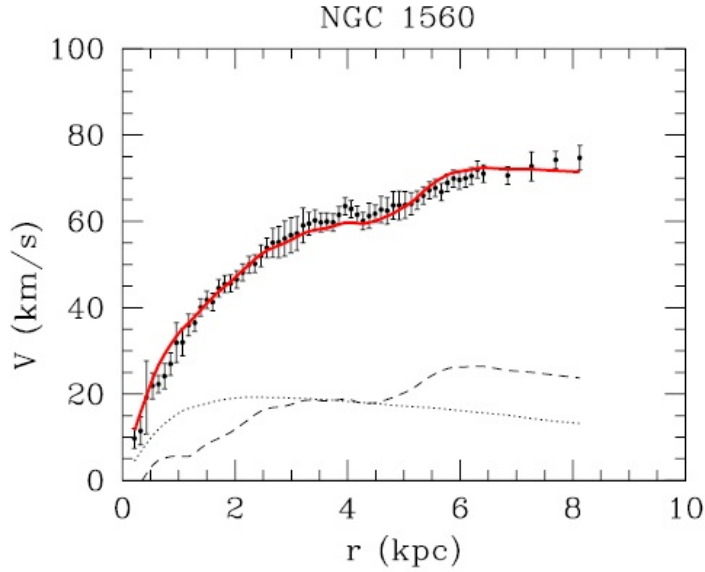


Figure 12. Rotation curve fit using MOND. The best-fit distance is 2.94 Mpc. Lines and symbols are like those in Fig. 10

FIG. 3. (Gentile et al., 2010) fit of NGC 1560, using MOND. In this graph, the “wobble” occurs where the stars, represented by the dotted line, give in to the H1 gas clouds, represented by the barred line, around 4 – 5 kpc .

In my approach, I first have to determine the model galaxy that fits best, using the parameters M and R , and then I can use M as a free parameter in order to create a perfect time bubble. In case of NGC 1560 however, it seems that in phase 1 two models partially fit the rotation curve. The first pure model fits NGC 1560 before the “wobble” the second pure model fits NGC 1560 after the “wobble”, see Fig.(4). Thus in my approach, the ‘constant Lagrangian’ model, the modeling indicates the underlying dynamics and the real world of unpredictable but observable mass distributions of stars and H1 gas clouds. The “wobble” divides NGC 1560 in two regions, which both follow their respective pure model relatively smoothly without being disturbed by that other part of the galaxy. The baryonic matter further away from the center than the H1 gas of producing “wobble” just behaves as if the bulge end where the “wobble” ends. The baryonic matter closer to the center than the H1 gas of producing “wobble” just behaves as if the H1 gas of the “wobble” is a perfect shell which doesn’t gravitate inside that shell. So the fact that two pure models can be made to partially fit the rotation curve actually reveals a lot of the underlying dynamics, reproducing known baryonic behavior under the influence of a Newtonian potential.

This fact, that one can only reasonably fit NGC 1560 by using two model fits, appeared to be the case for most galaxies. The shift from one model fit to the other model fit always follows the shift from stars dominated mass distribution to H1 gas dominated mass distribution.

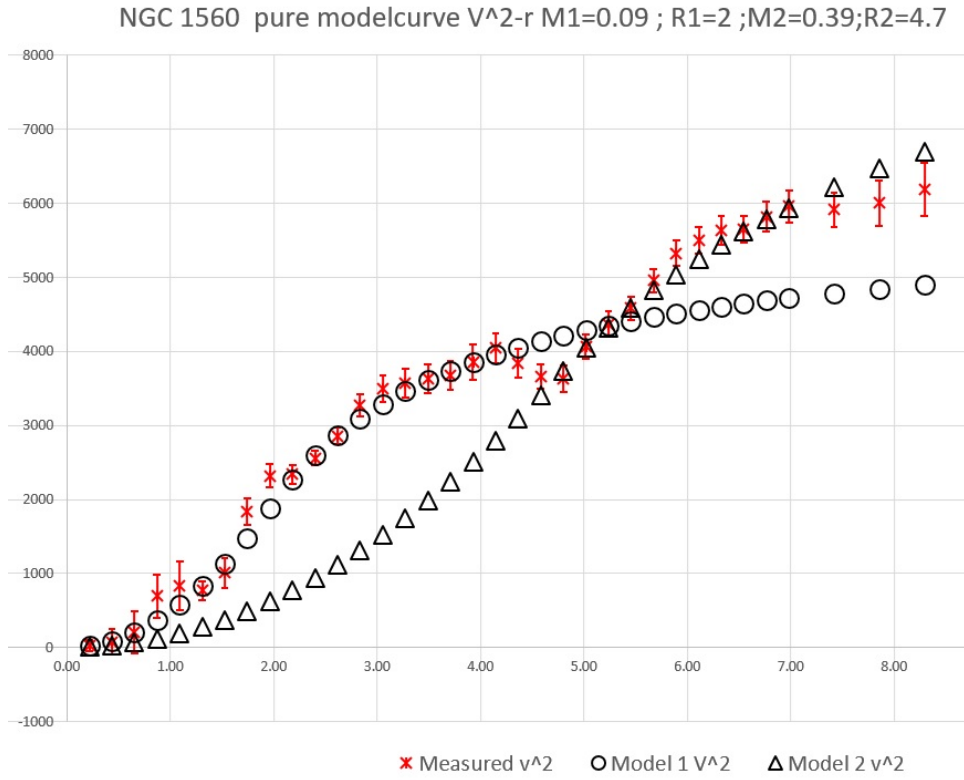


FIG. 4. NGC1560, V_{orb}^2 against r . Pure model 1 with $M1=0.09$ and $R1=2$. Pure model 2 with $M2=0.39$ and $R2=4.7$.

IV. THE STARS TO GAS SHIFT IN THE ROTATION CURVE OF SOME OTHER GALAXIES

While analyzing the SPARC database, this shift proved quite general. In the following I will give some examples. First I give the dual plot of the rotation curve, then I compare the result against the mass distribution made available by SPARC.

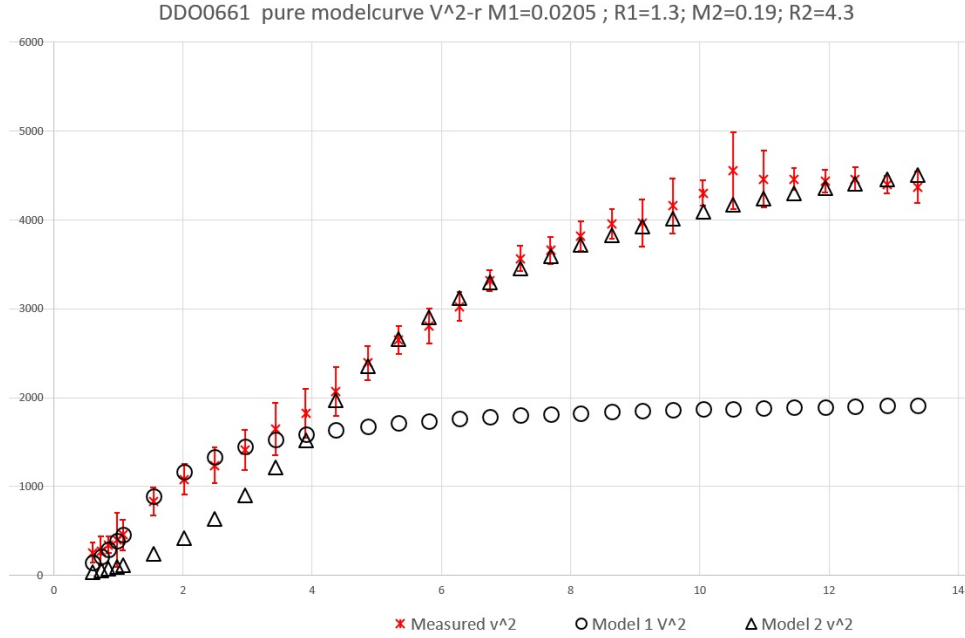


FIG. 5. DDO0661, V_{orb}^2 against r .

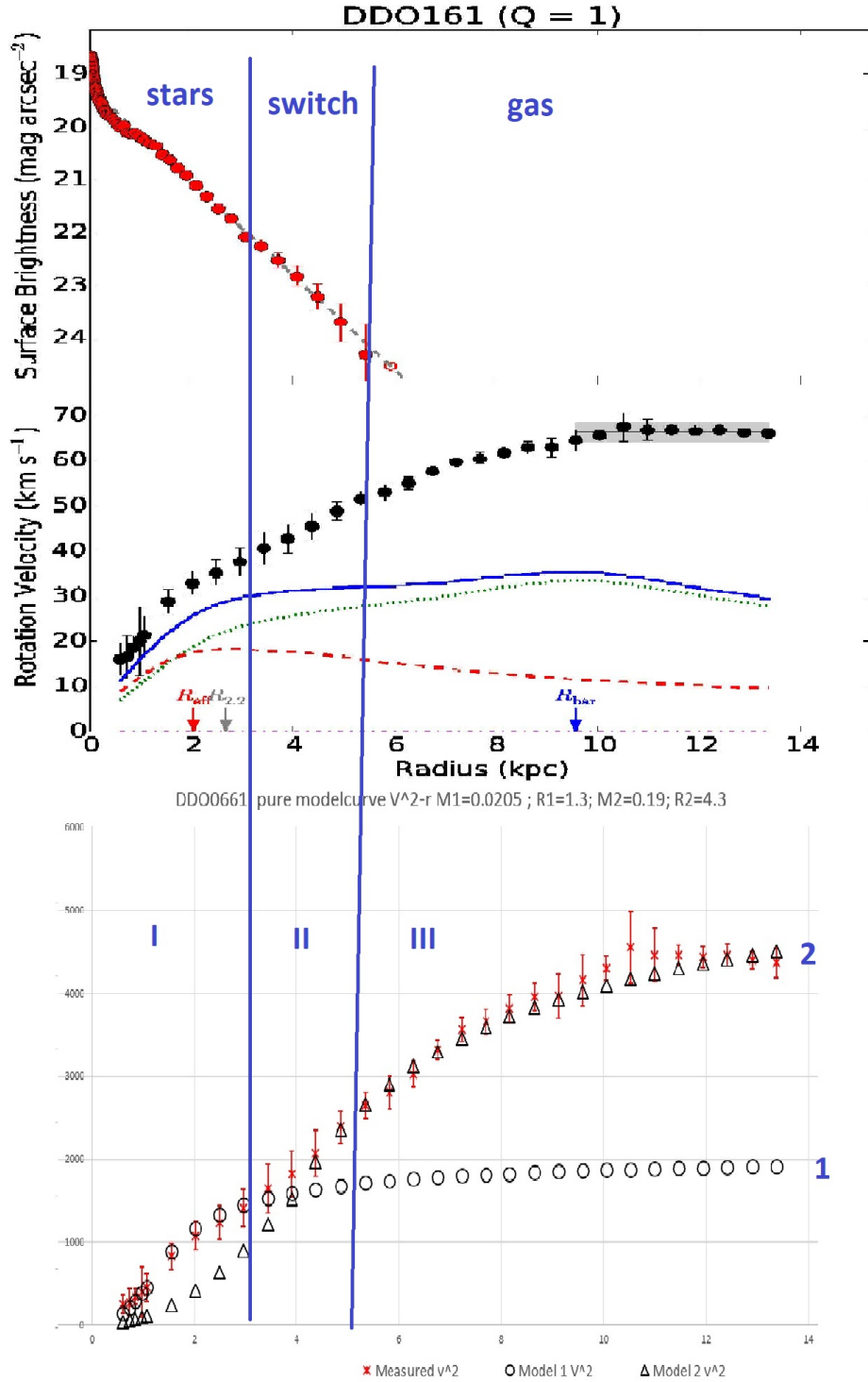


FIG. 6. DDO0661, V_{orb}^2 against r , and the stars and gas mass distribution plot. The red dots are the luminous stars, the dotted line the gas contribution to the mass and the red bars line represent the stars contribution to the velocity curved, assuming the virial theorem.

NGC 2403 pure modelcurve V^2 - r $M_1= 0.23$; $R_1=1.6$; $M_2=0.058$; $R_2=0.65$

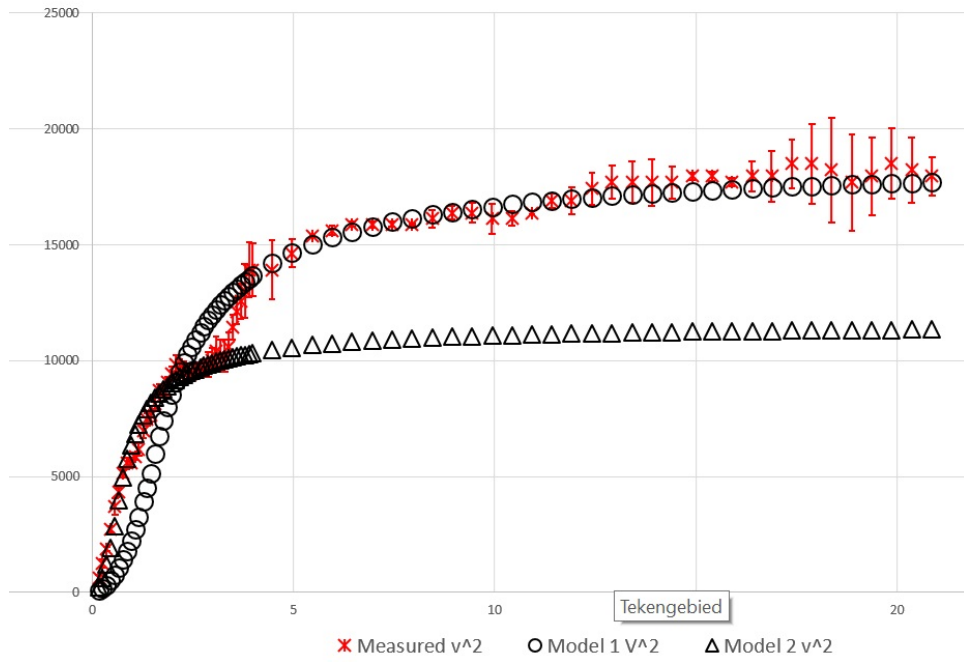


FIG. 7. NGC2403, V_{orb}^2 against r .

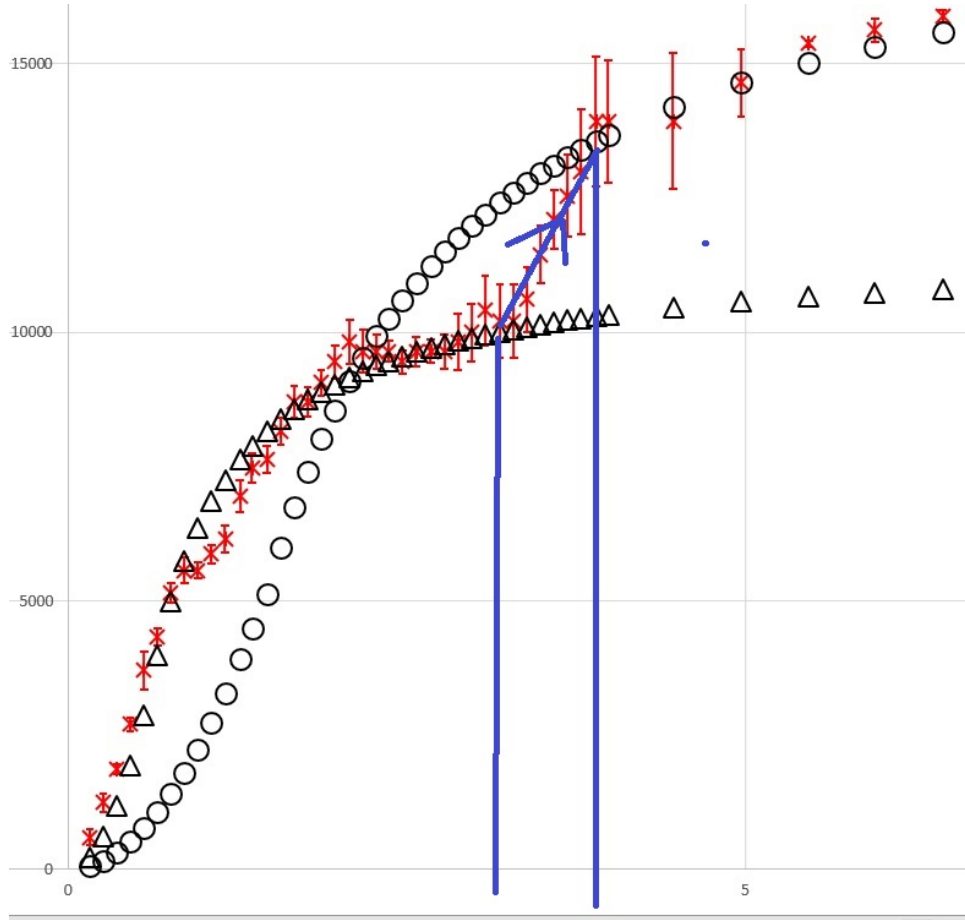


FIG. 8. Detail of NGC2403, V_{orb}^2 against r .

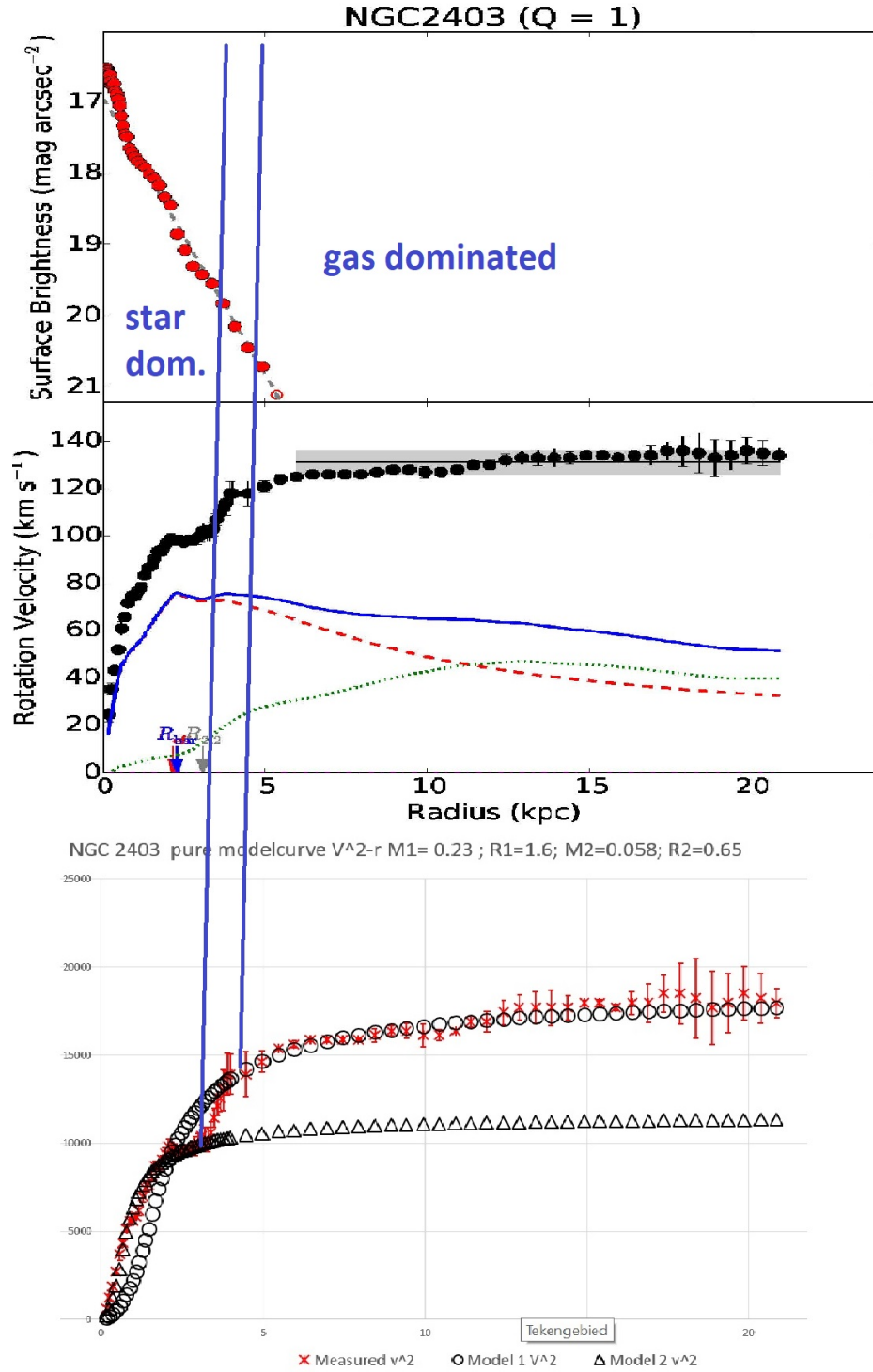


FIG. 9. Analysis of NGC2403, V_{orb}^2 against r .

UGCA444 pure modelcurve V^2-r $M1=0.0065$; $R1=0.7$; $M2=0.018$; $R2=1.2$

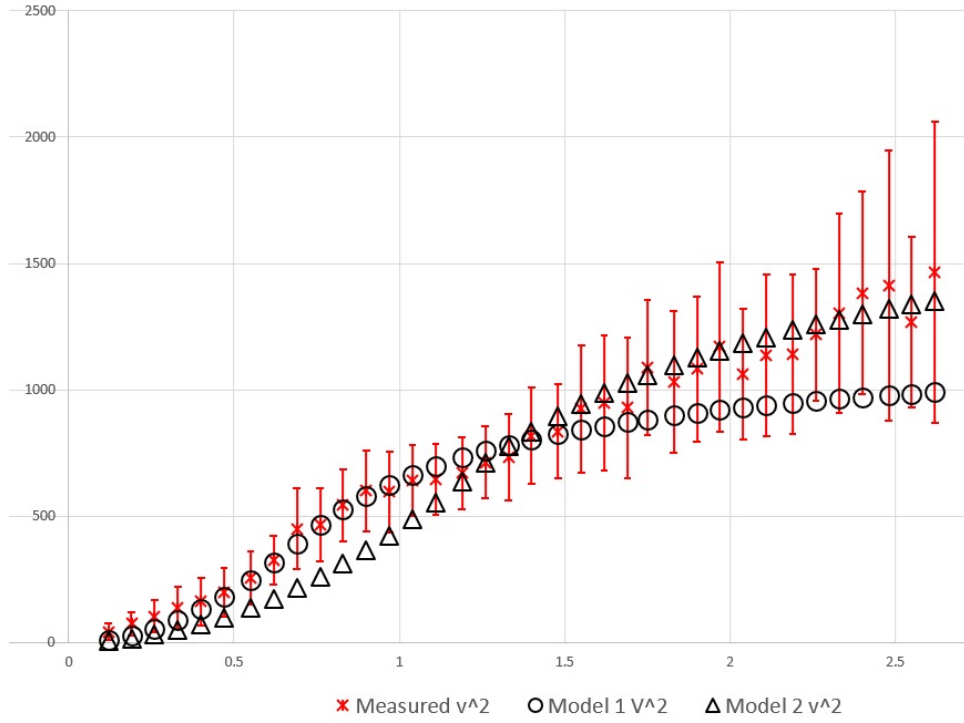


FIG. 10. UGCA444, V_{orb}^2 against r .

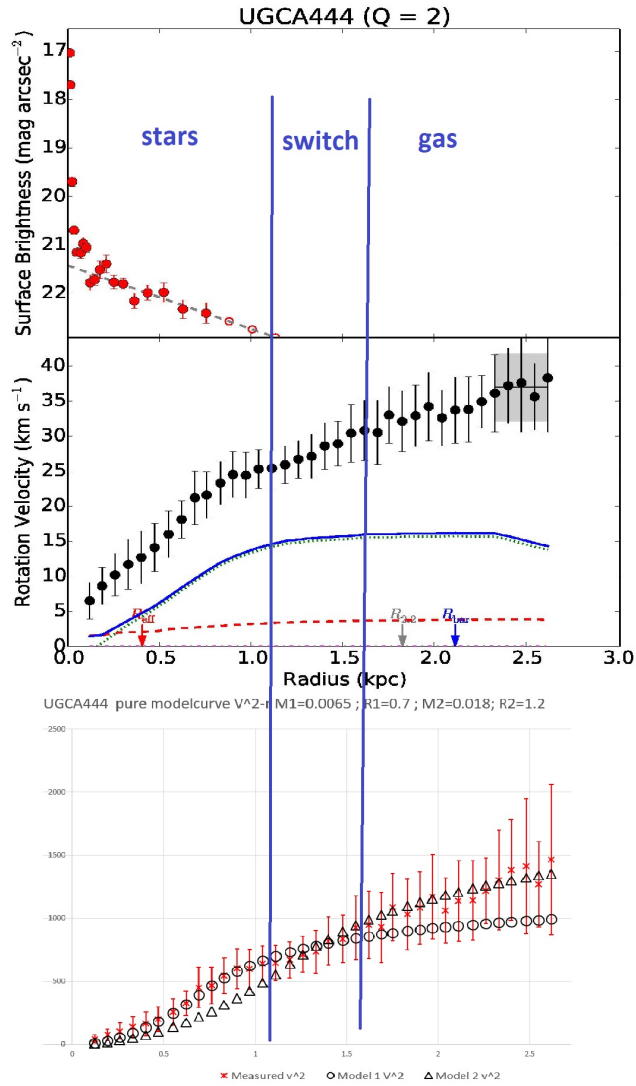


FIG. 11. Analysis of UGCA444, V_{orb}^2 against r .

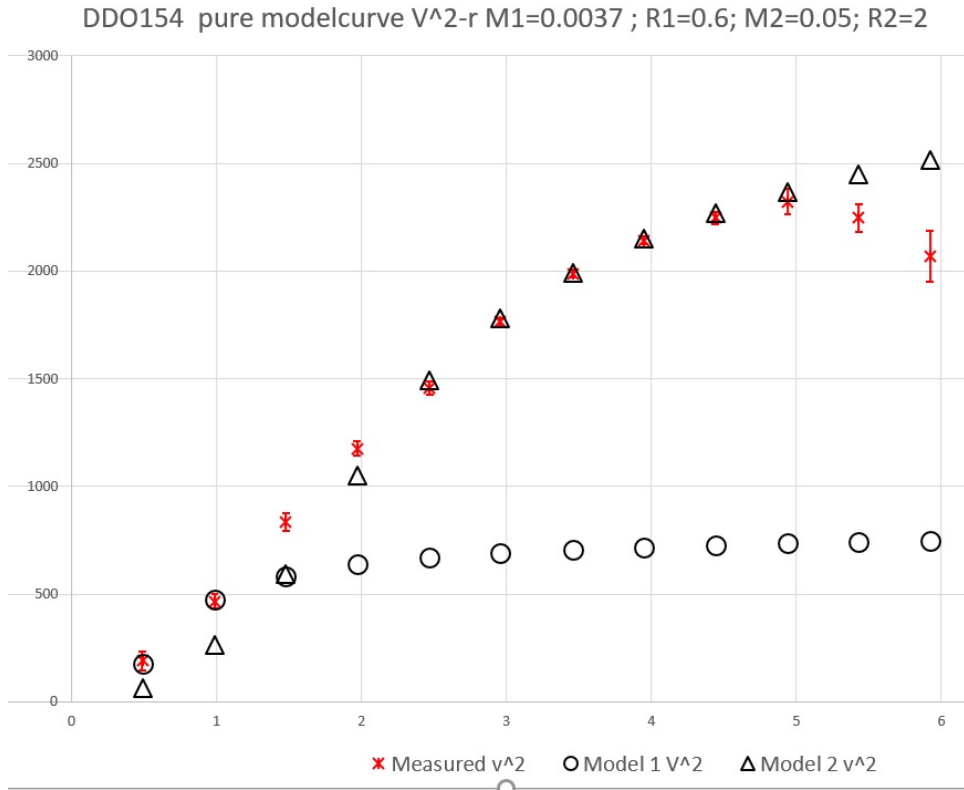


FIG. 12. DDO154, V_{orb}^2 against r .

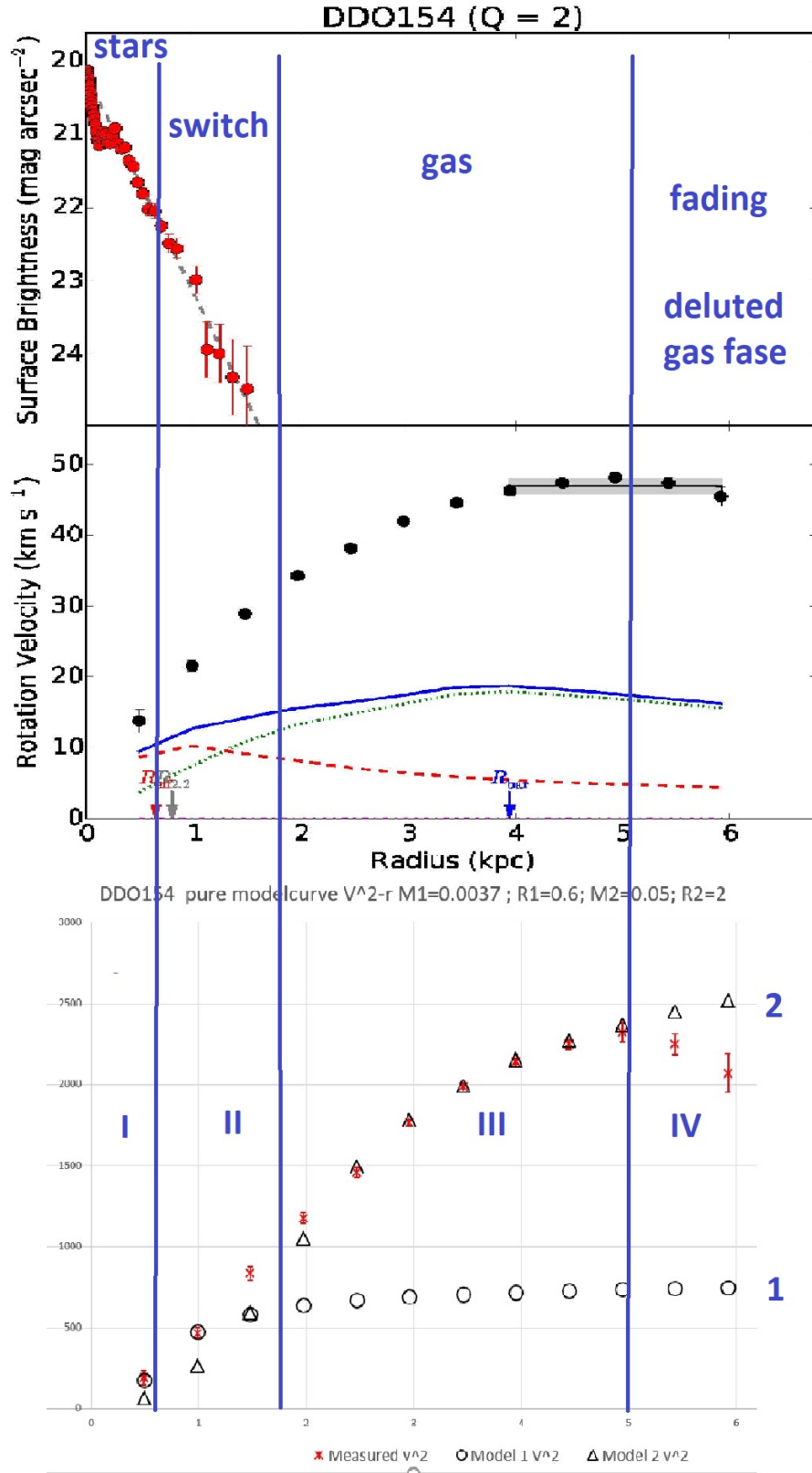


FIG. 13. Analysis of DDO154, V_{orb}^2 against r .

The following two fits of D613-7 demonstrate the difficulty of fitting the rotation curve with one model curve, see Fig.(14), and the ‘solution’ of fitting the rotation curve with two model curves, while allowing the measured curve to move from the first model curve to the second model curve during the shift from the stars dominated to the gas dominated region, see Fig.(15). The shift is loosely connected to the shift from stars to gas region of the galaxy, as can be seen in Fig.(16).

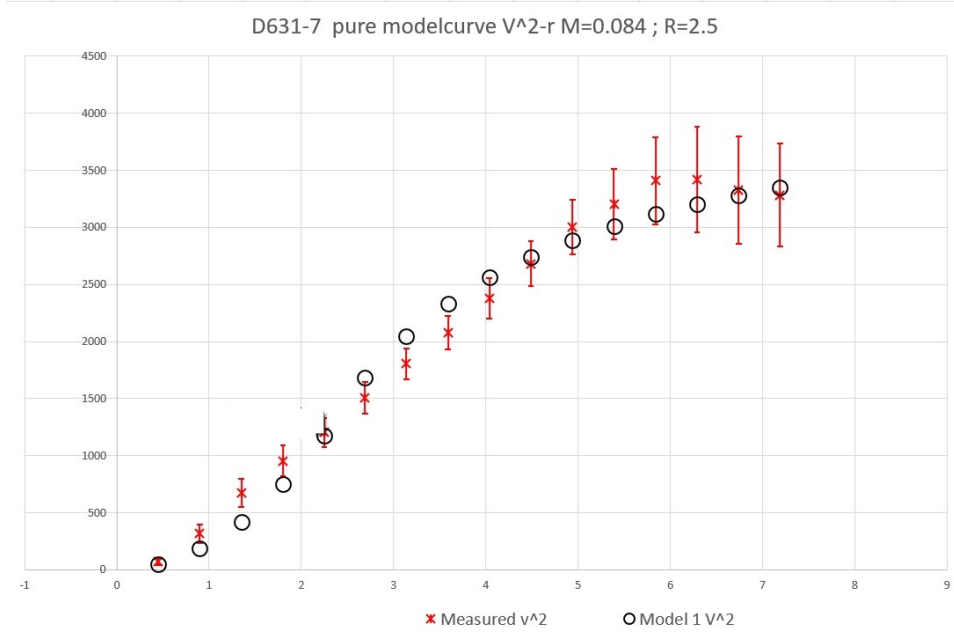


FIG. 14. D613-7 single fit, V_{orb}^2 against r .

D631-7 pure modelcurve V^2-r $M1=0.028$; $R1=1.5$; $M2=0.053$; $R2=1.7$

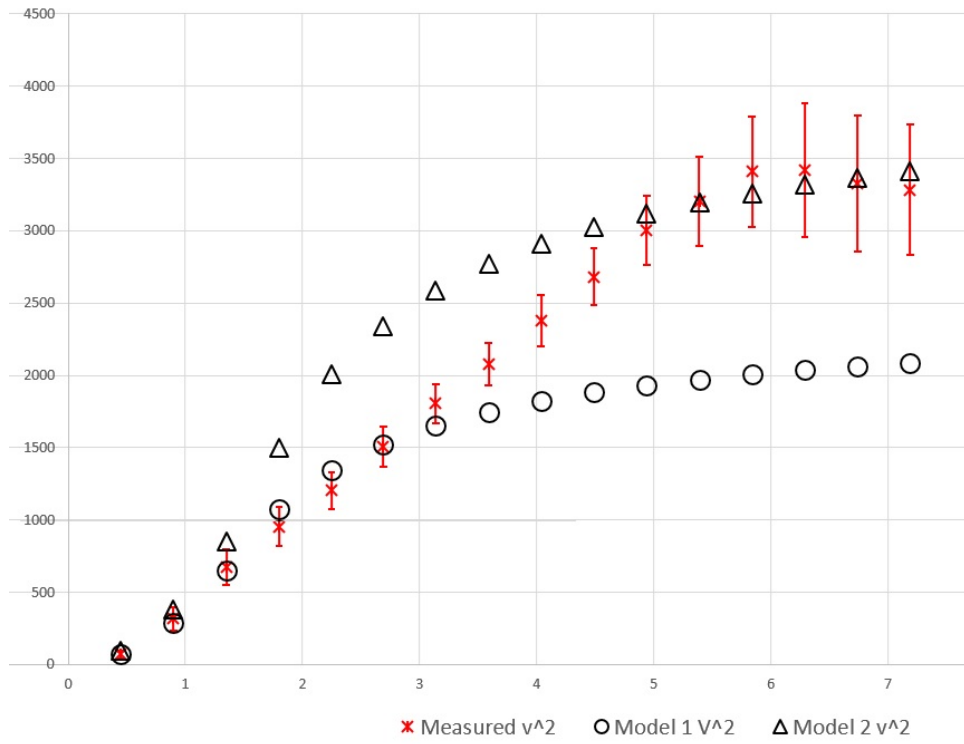


FIG. 15. D613-7 dual fit, V_{orb}^2 against r .

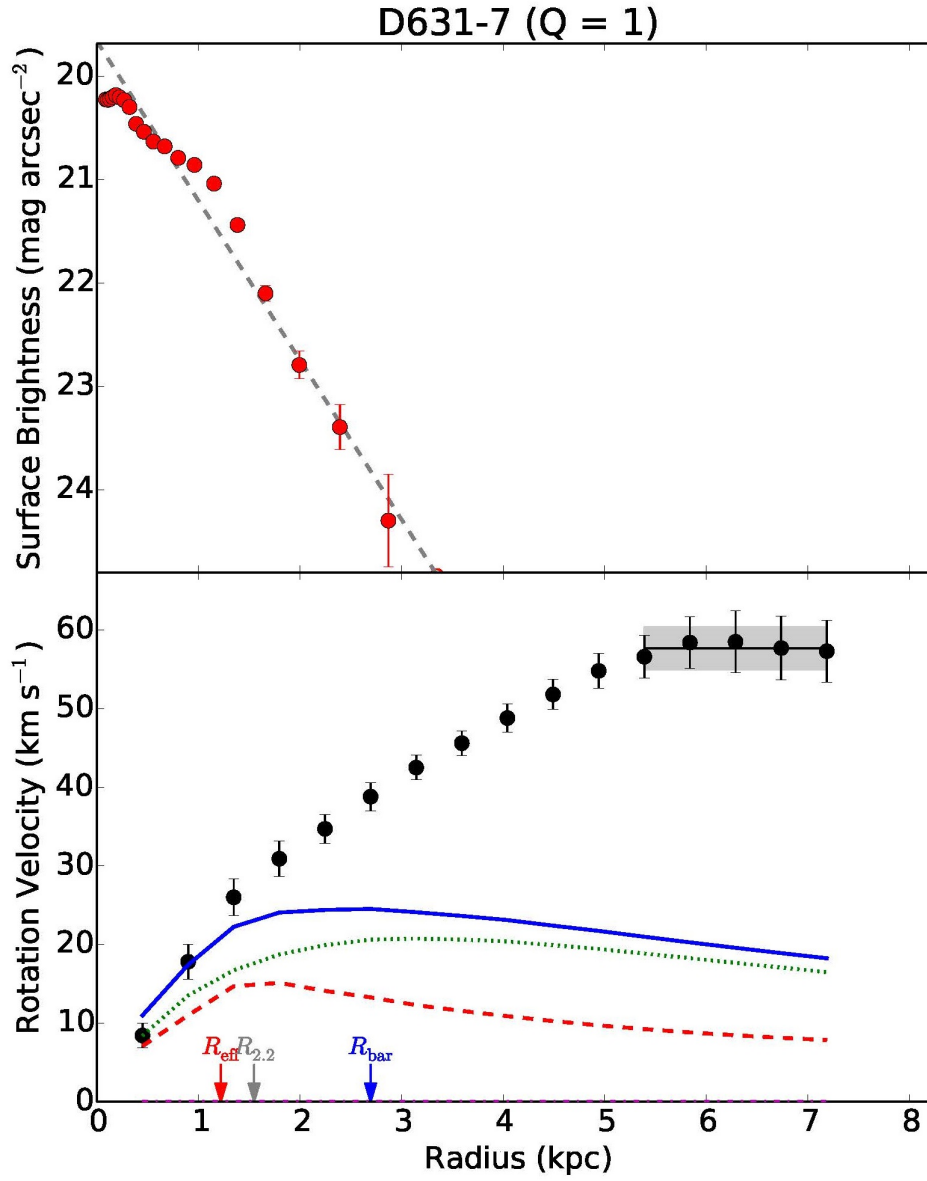


FIG. 16. D613-7 mass distribution from the SPARC database.

V. SOME MORE ROTATION CURVE FITS: F583-1, F579V1 AND U11648

In this section, I present the ‘constant Lagrangian’ rotation curve dual fits of some 20 other galaxies of the [SPARC database](#), including the error margins, as provided by (Lelli et al., 2016). It is to the reader to compare the results with the mass distribution graphs of SPARC (from the [MassModels-LTG.zip](#) file).

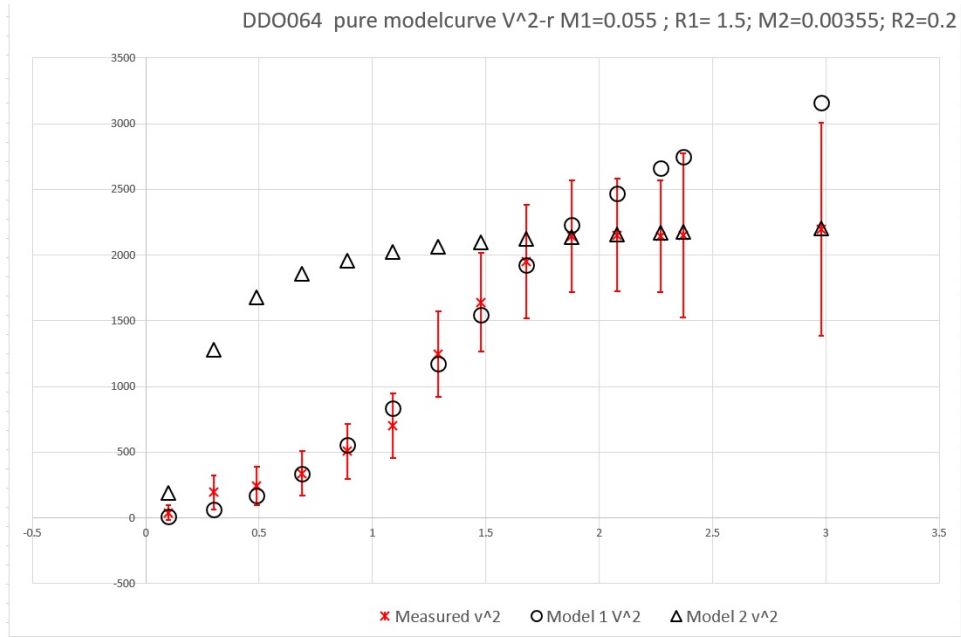


FIG. 17. DDO064, V_{orb}^2 against r

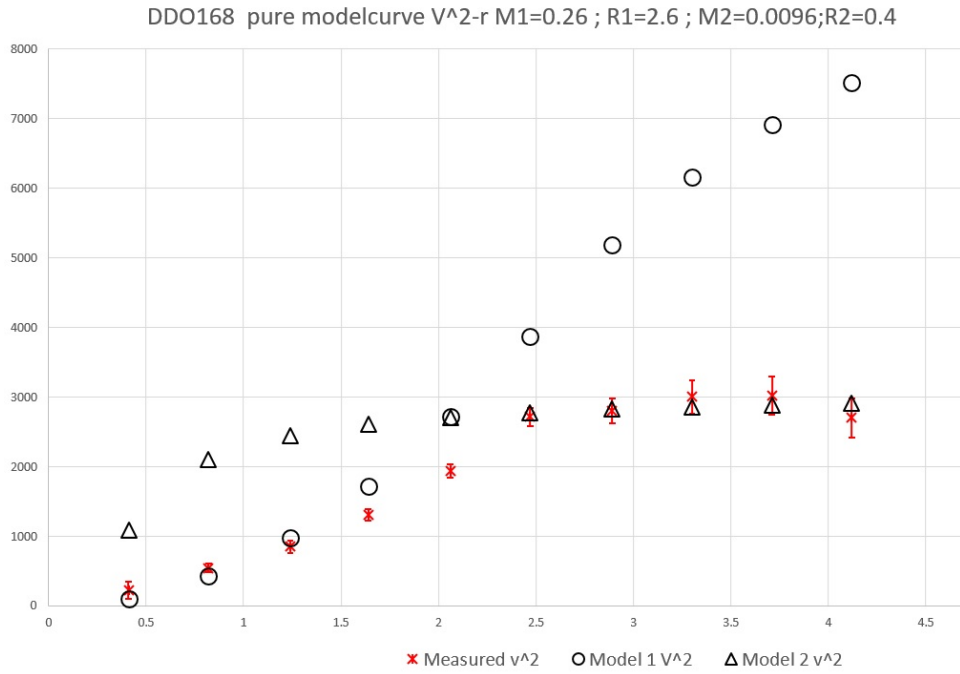


FIG. 18. DDO168, V_{orb}^2 against r

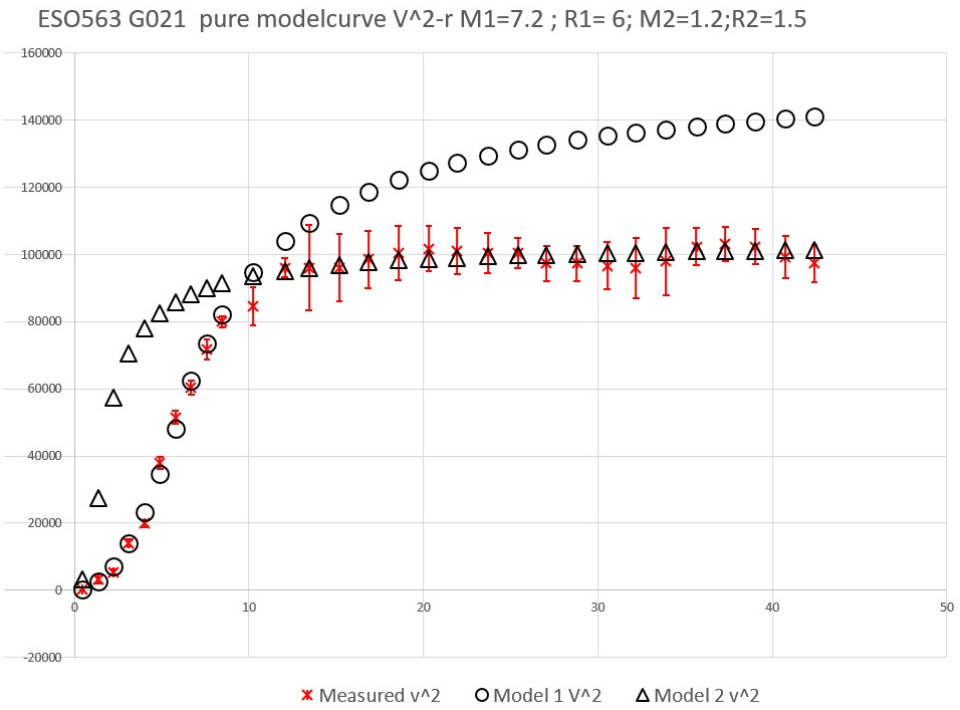


FIG. 19. ESO563, V_{orb}^2 against r

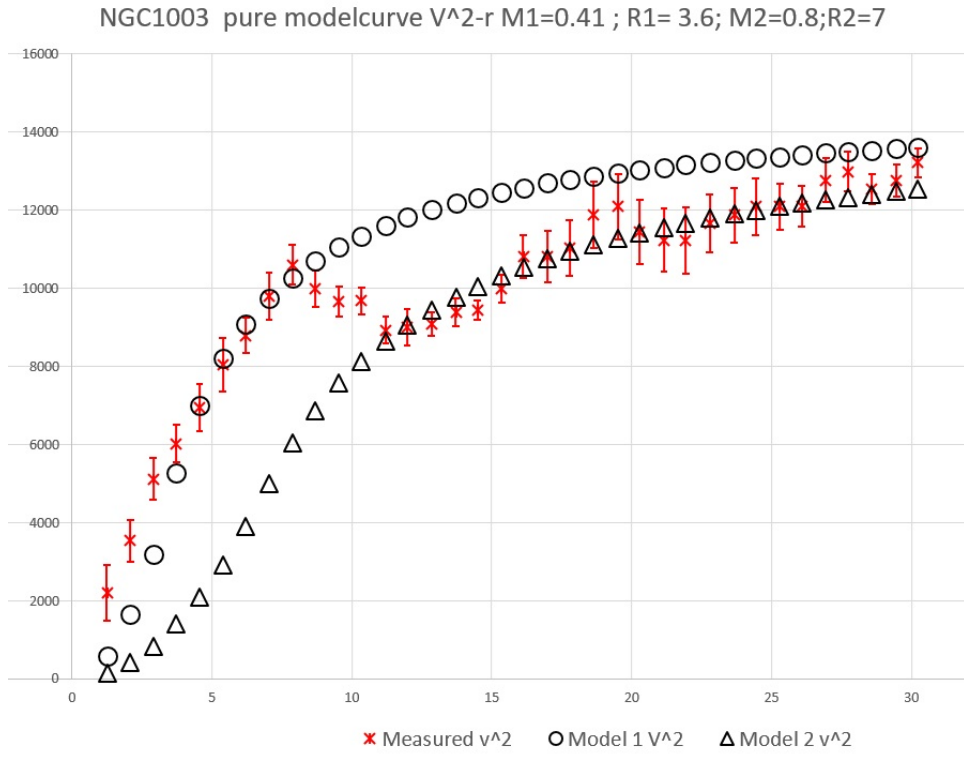


FIG. 20. NGC1003, V_{orb}^2 against r

NGC2366 pure modelcurve V^2-r $M1=0.045$; $R1=1.6$; $M2=0.0062$; $R2=0.3$

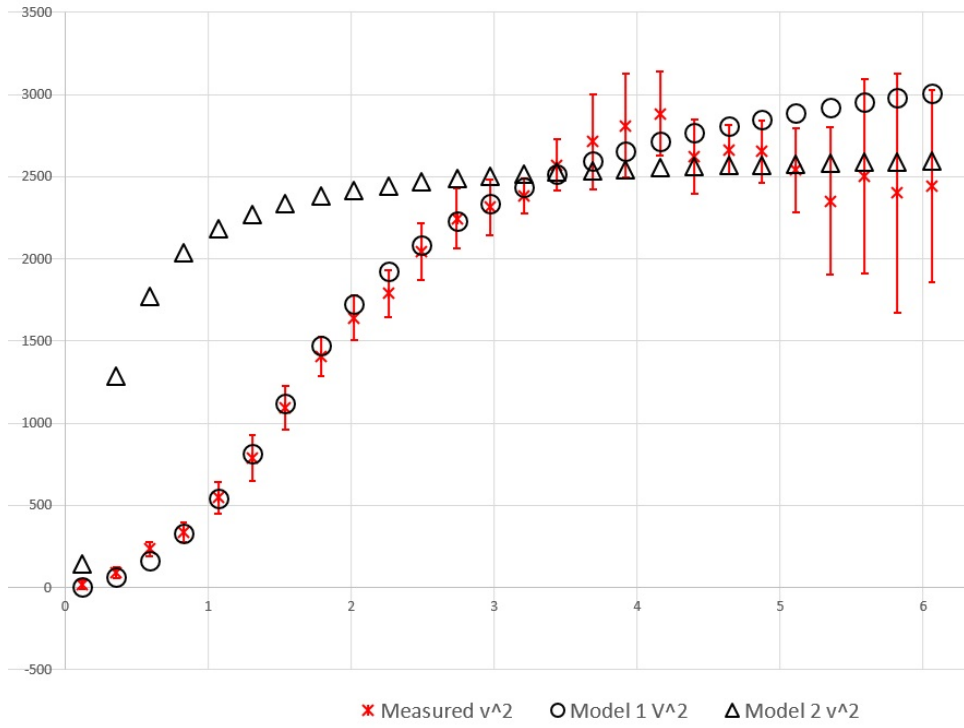


FIG. 21. NGC2366, V_{orb}^2 against r

NGC4100 pure modelcurve V^2-r $M1=1.17$; $R1=2.9$; $M2=0.1$; $R2=0.5$

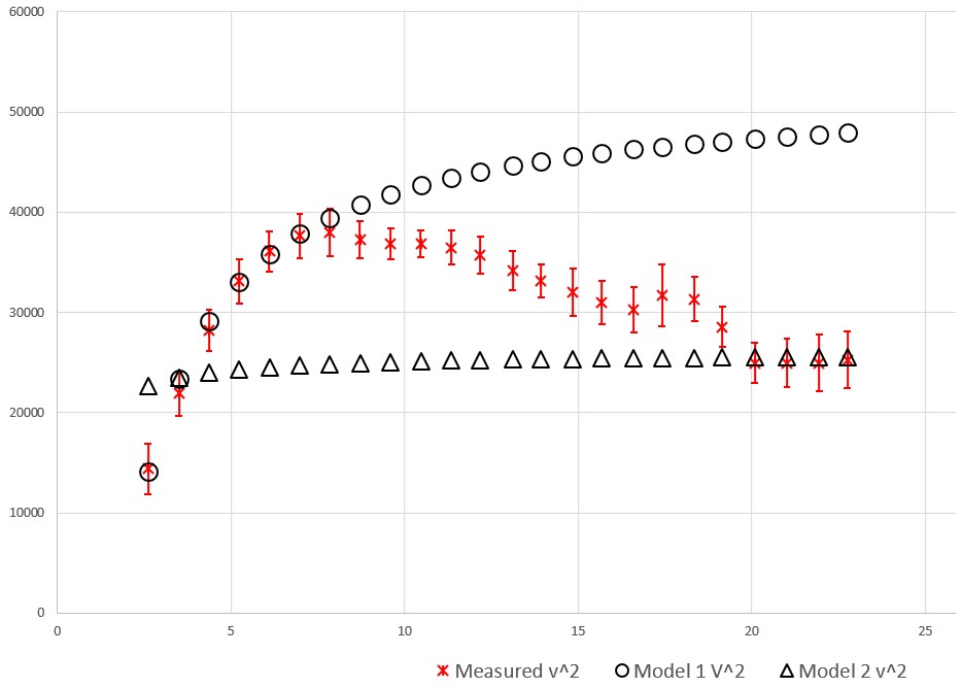


FIG. 22. NGC4100, V_{orb}^2 against r

NGC4183 pure modelcurve V^2-r $M1=0.48$; $R1=3.5$; $M2=0.049$; $R2=0.5$

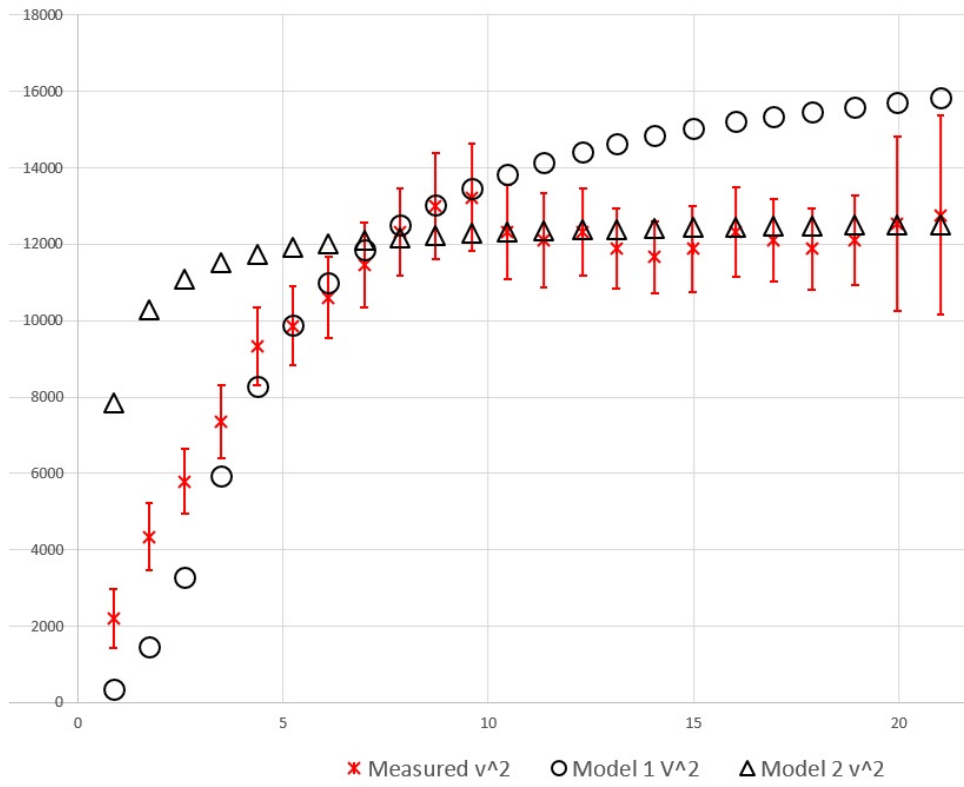


FIG. 23. NGC4183, V_{orb}^2 against r

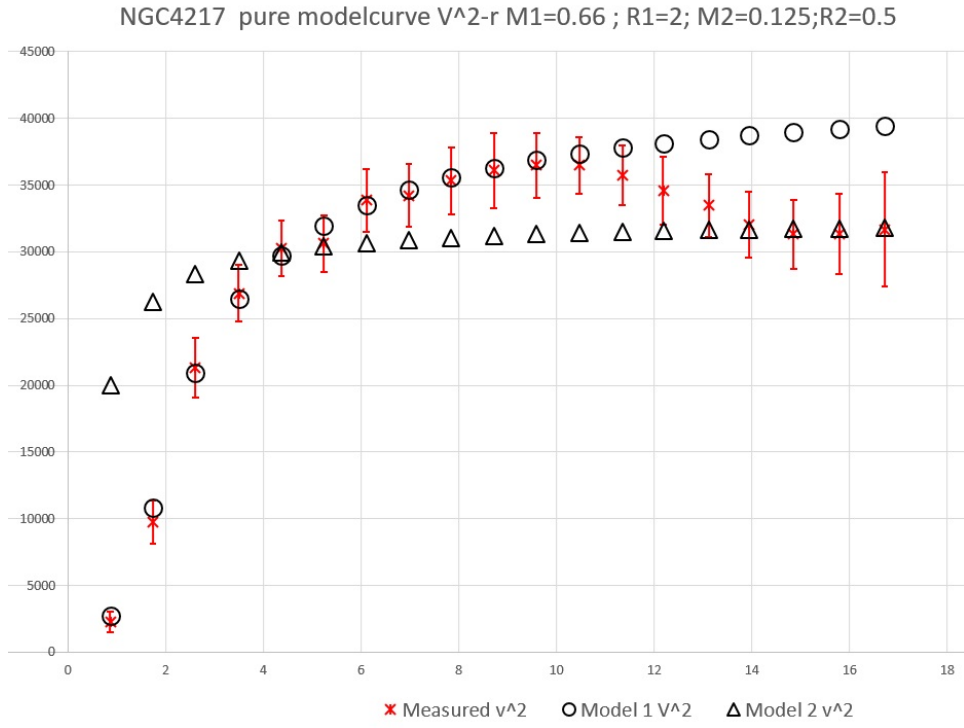


FIG. 24. NGC4217, V_{orb}^2 against r

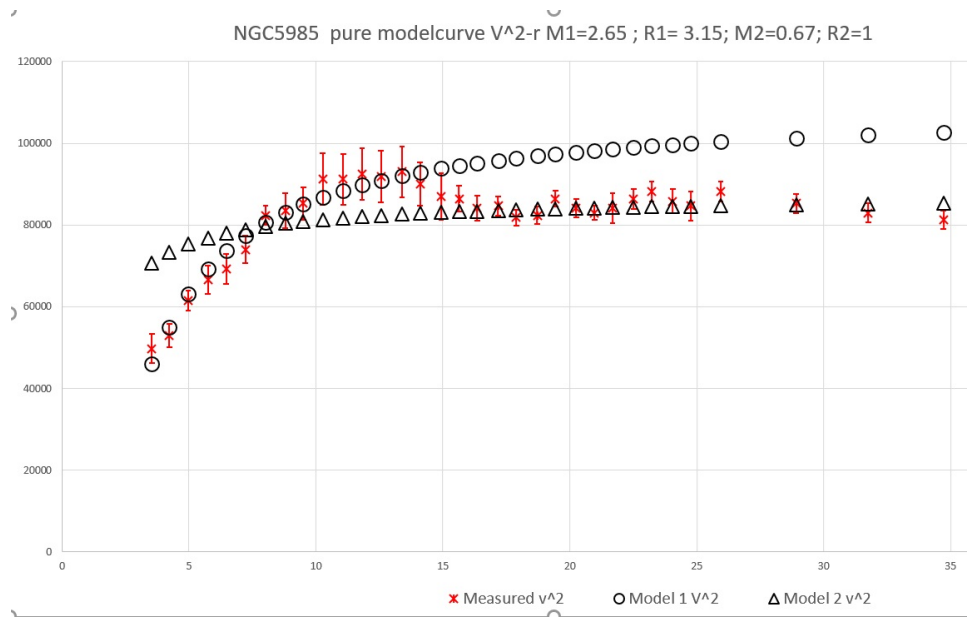


FIG. 25. NGC5985, V_{orb}^2 against r

UGC128 pure modelcurve V^2-r $M_1=0.43$; $R_1= 3.5$; $M_2=0.133$; $R_2=1$

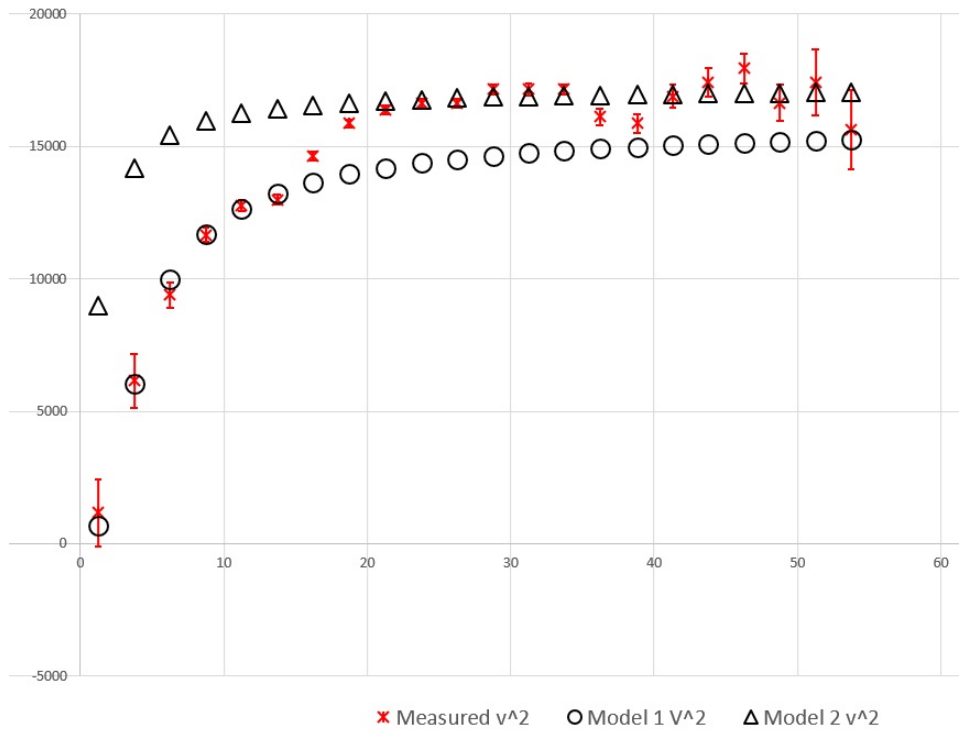


FIG. 26. UGC128, V_{orb}^2 against r

UGC06446 pure modelcurve V^2-r $M1=0.034$; $R1=0.8$; $M2=0.033$; $R2=0.6$

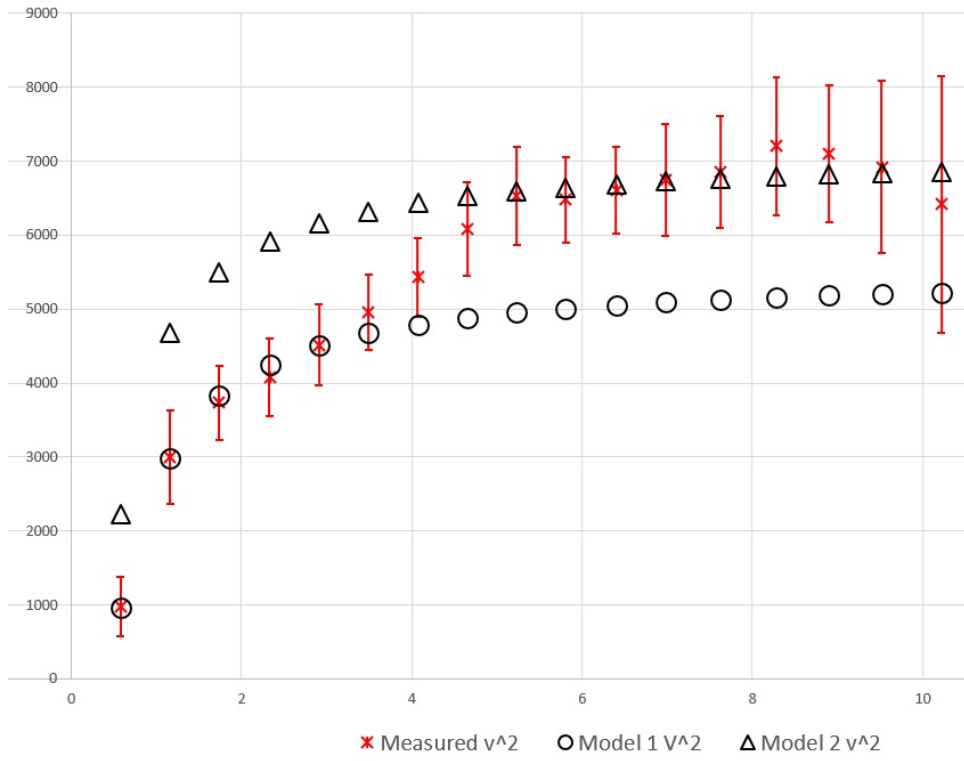


FIG. 27. UGC06446, V_{orb}^2 against r

UGC 07524 pure modelcurve V^2-r M1=0.022 ; R1=1.05; M2=0.233; R2=3.5

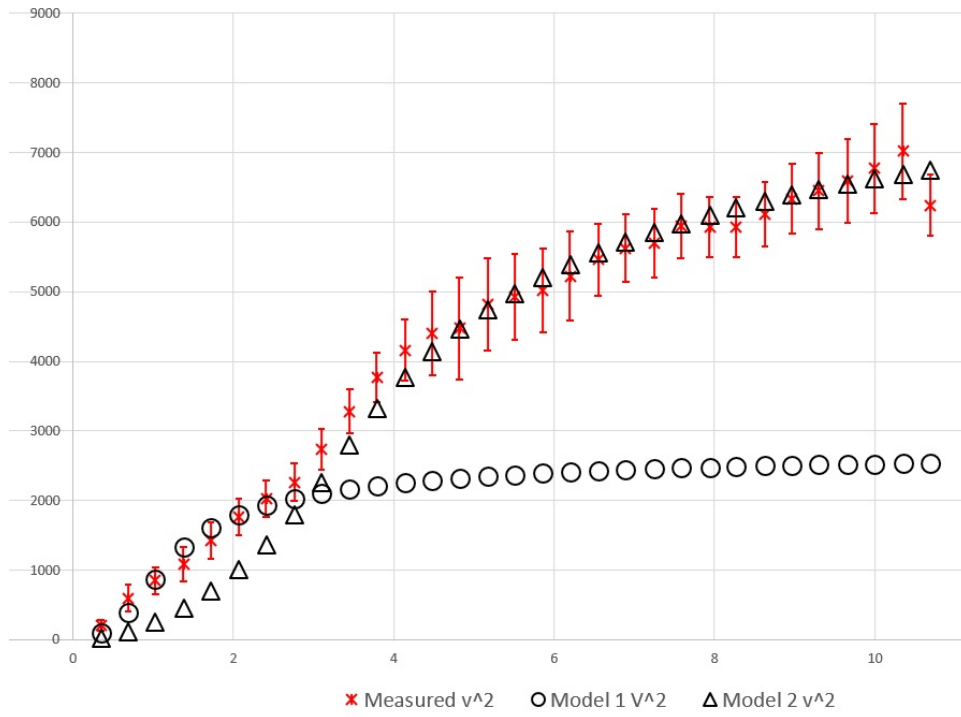


FIG. 28. UGC07524, V_{orb}^2 against r

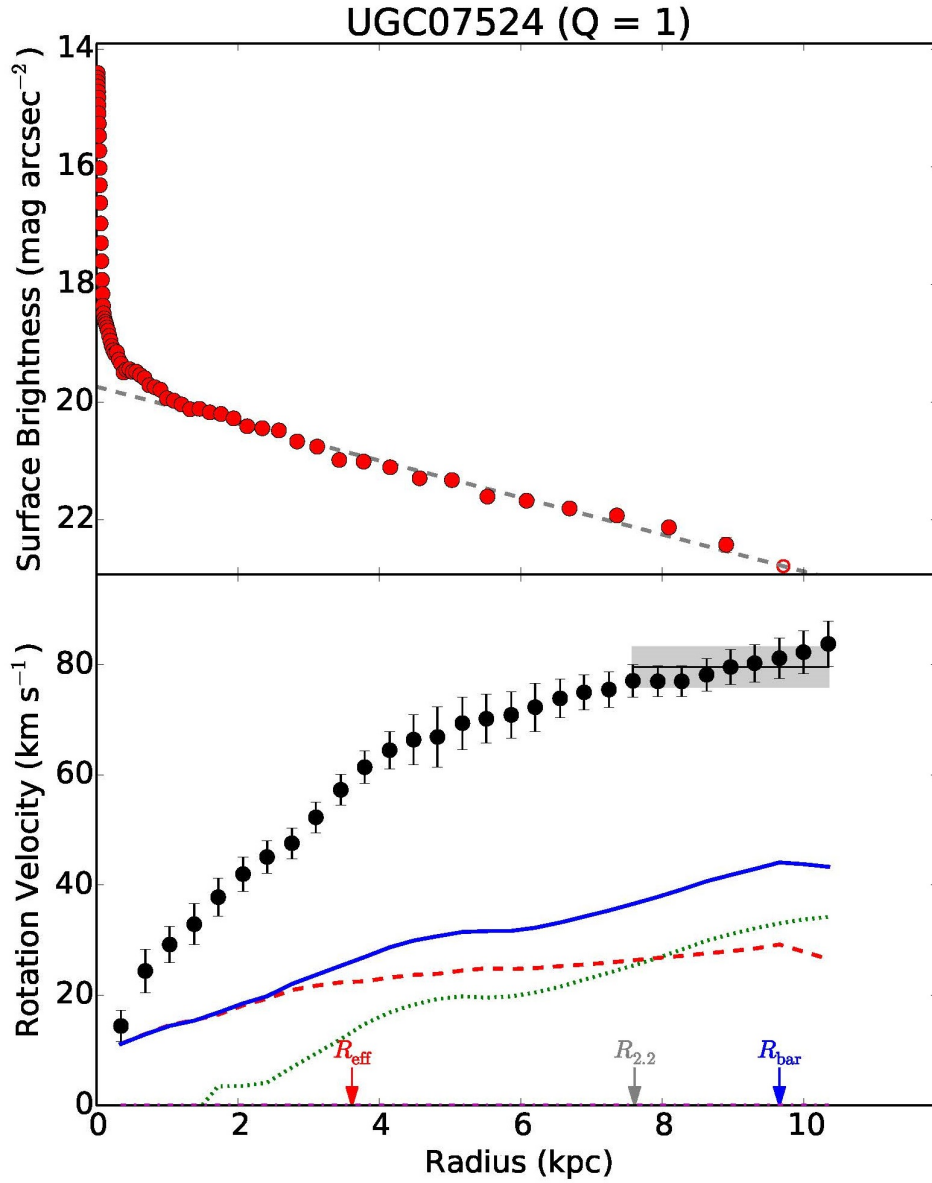


FIG. 29. UGC07524 mass distribution from the SPARC database

UGC11820 pure modelcurve V²-r M1=0.045 ; R1=1;M2=0.41;R2=5.7

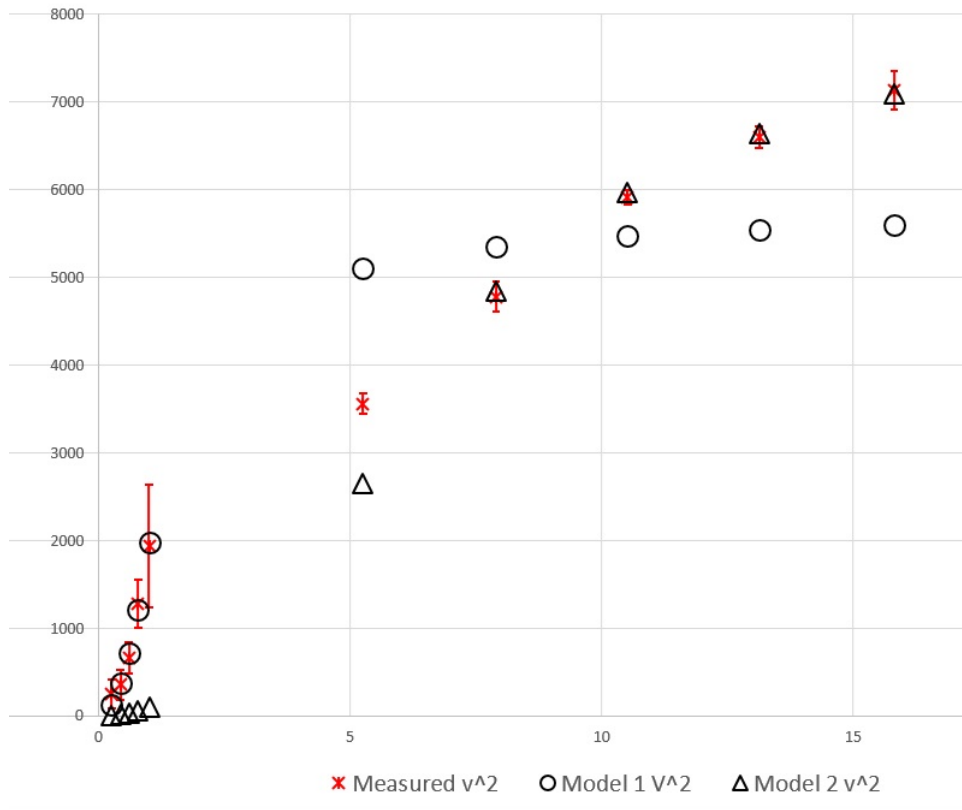


FIG. 30. UGC11820, V_{orb}^2 against r

UGC12632 pure modelcurve V^2-r $M1=0.038$; $R1=1.4$; $M2=0.135$; $R2=2.7$

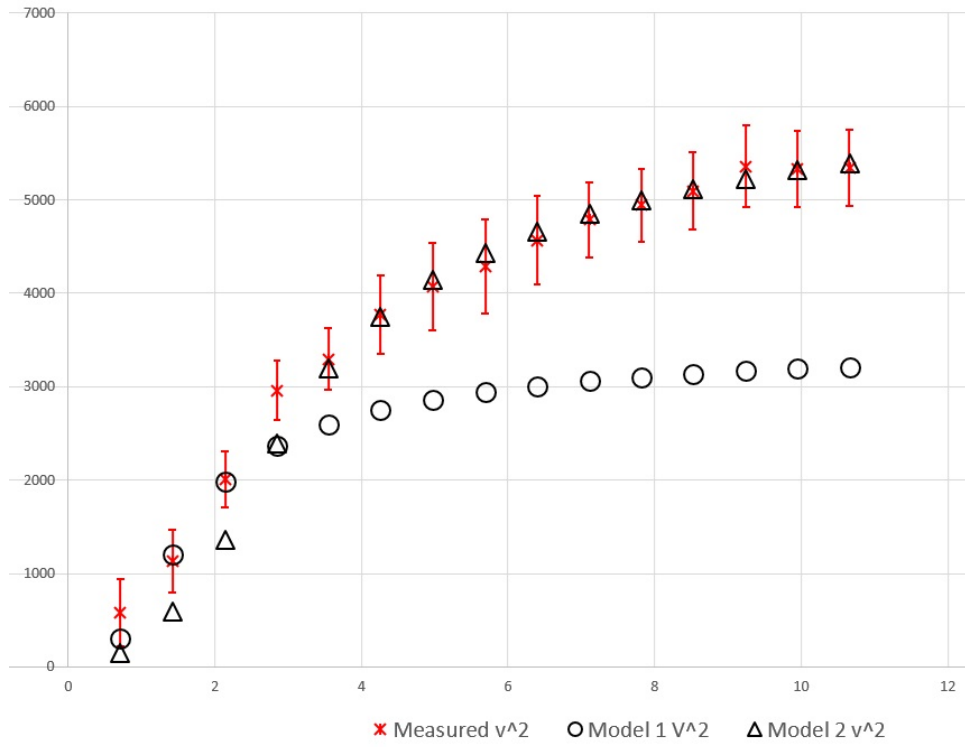


FIG. 31. UGC12632, V_{orb}^2 against r

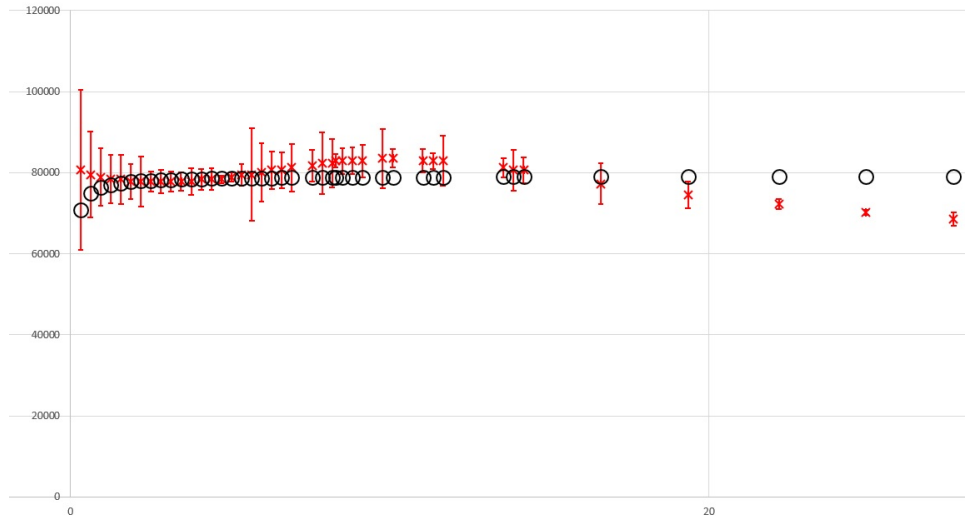


FIG. 32. UGC09133 from 0 to 20 kpc, V_{orb}^2 against r

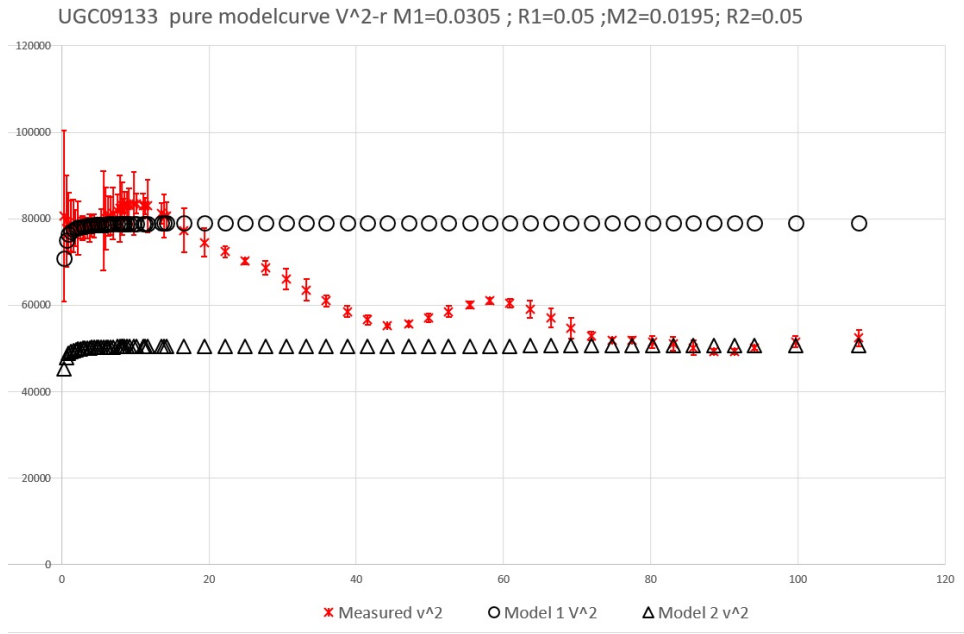


FIG. 33. UGC09133 from 0 to 120 kpc, V_{orb}^2 against r

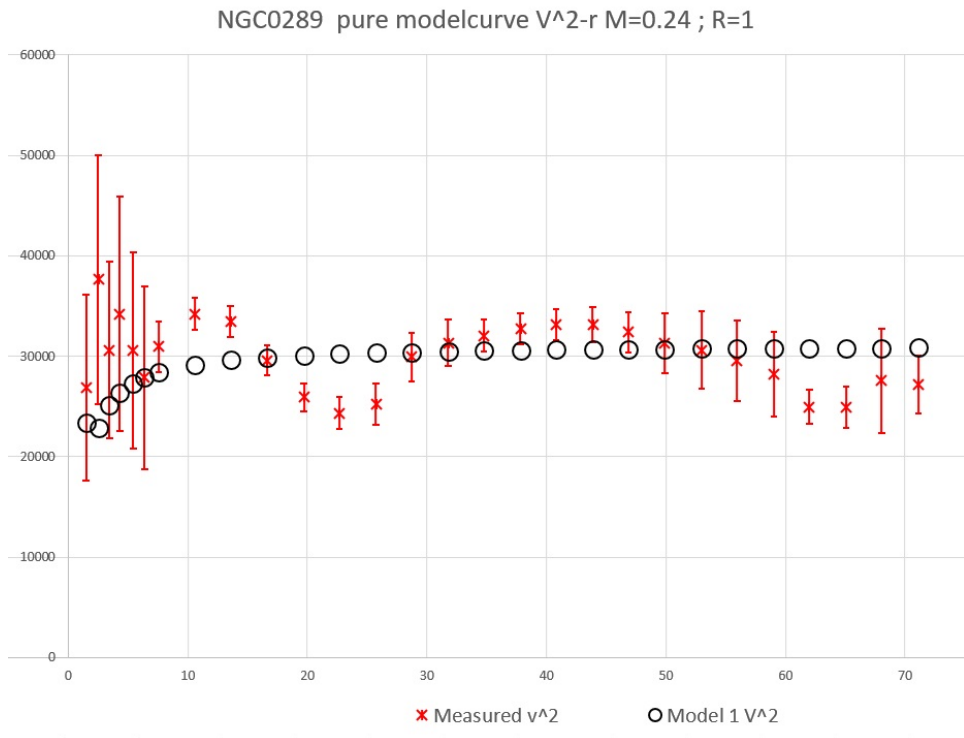


FIG. 34. NGC0289, V_{orb}^2 against r

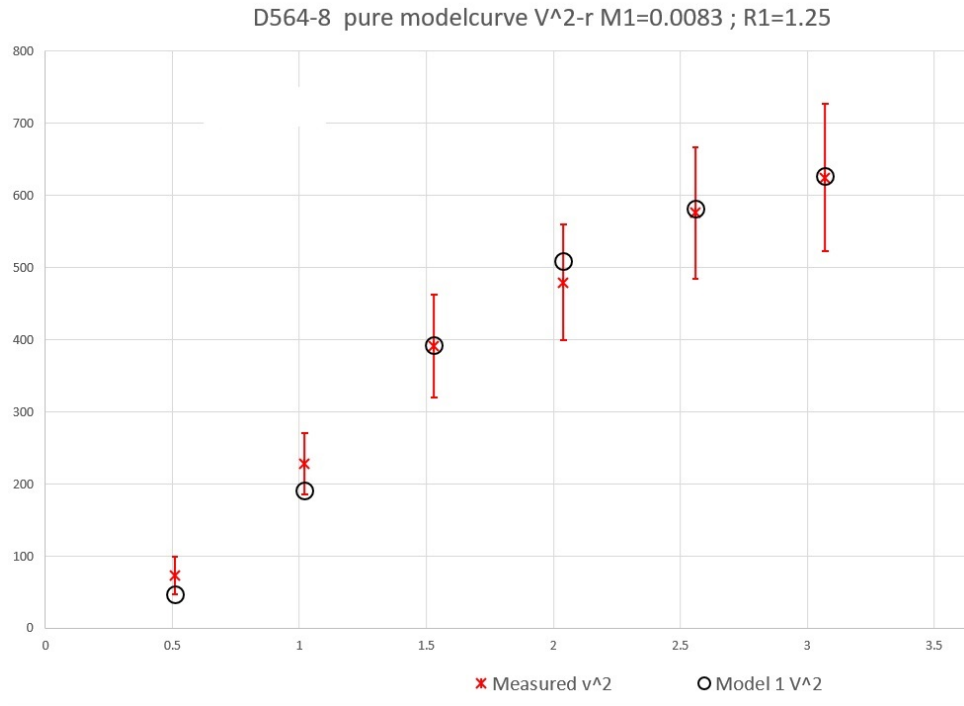


FIG. 35. D564-8, V_{orb}^2 against r

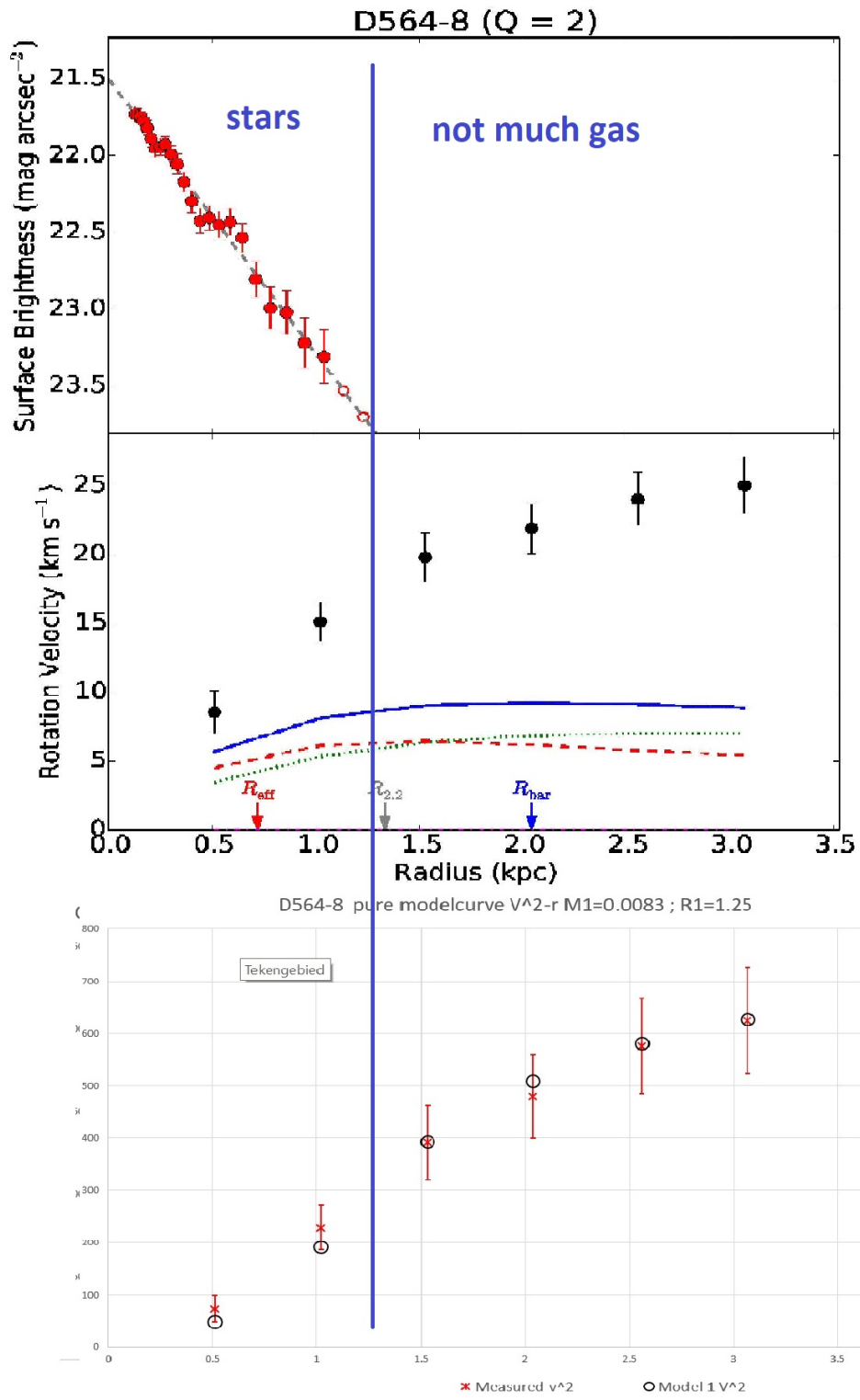


FIG. 36. D564-8 analysis, V_{orb}^2 against r

REFERENCES

- Ashby, N. (2002, May). Relativity and the global positioning system. *Physics Today* 55(5), 41–47.
- de Haas, E. P. J. (2018a). A ‘constant lagrangian’ model for galactic dynamics in a geodetic approach towards the galactic rotation dark matter issue. *Preprint on viXra.org:Astrophysics*. [vixra:1804.0298](https://arxiv.org/abs/1804.0298).
- de Haas, E. P. J. (2018b). Fitting some galaxy rotation curves using the ‘constant lagrangian’ model for galactic dynamics. *Preprint on viXra.org:Astrophysics*. [vixra:1804.0386](https://arxiv.org/abs/1804.0386).
- de Haas, E. P. J. (2018c). Fitting the ngc 1560 rotation curve and other galaxies in the ‘constant lagrangian’ model for galactic dynamics. *Preprint on viXra.org:Astrophysics*. [vixra:1804.0328](https://arxiv.org/abs/1804.0328).
- Delva, P. and J. Lodewyck (2013). Atomic clocks: new prospects in metrology and geodesy. In *Workshop on Relativistic Positioning Systems and their Scientific Applications Brdo, Slovenia, September 19-21, 2012*. arXiv:1308.6766 [physics.atom-ph].
- Gentile, G., M. Baes, B. Famaey, and K. Van Acoleyen (2010). Mass models from high-resolution h i data of the dwarf galaxy ngc 1560. *Monthly Notices of the Royal Astronomical Society* 406(4), 2493–2503.
- Hećimović, Ž. (2013). Relativistic effects on satellite navigation. *Tehnički vjesnik* 20(1), 195–203.
- Kopeikin, S. M., I. Y. Vlasov, and W. B. Han (2017). The normal gravity field in relativistic geodesy. *ArXiv e-prints*. arXiv:1708.09456 [gr-qc].
- Lelli, F., S. S. McGaugh, and J. M. Schombert (2016, December). SPARC: Mass Models for 175 Disk Galaxies with Spitzer Photometry and Accurate Rotation Curves. *The Astronomical Journal* 152, 157.
- Mayrhofer, R. and R. Pail (2012). Future satellite gravity field missions: Feasibility study of post-newtonian method. In S. Kenyon (Ed.), *Geodesy for Planet Earth*, Volume 136 of *International Association of Geodesy Symposia*, pp. 231–238. Springer International Publishing. Switzerland.
- McGaugh, S. S. (2005). The baryonic tully-fisher relation of galaxies with extended rotation curves and the stellar mass of rotating galaxies. *The Astrophysical Journal* 632, 859–871. [arXiv:astro-ph/0506750v2](https://arxiv.org/abs/astro-ph/0506750v2).

- McGaugh, S. S., V. C. Vera C. Rubin, and W. J. G. de Blok (2001). High-resolution rotation curves of low surface brightness galaxies. i. data. *The Astronomical Journal* 122(5), 2381.
- Mercier, C. (2015). Calculation of the apparent mass of the universe. [Website access](#) (accessed on April, 14, 2018).
- Milgrom, M. (1983). A modification of the newtonian dynamics - implications for galaxies. *The Astrophysical Journal* 270, 371–387. [Astronomy Abstract Service pdf](#).
- Ruggiero, M. L., D. Bini, A. Gerialico, and A. Tartaglia (2008). Emission versus fermi coordinates: applications to relativistic positioning systems. *Classical and Quantum Gravity* 25(20), 205011. arXiv:0809.0998 [gr-qc].

